

Effect of Na substitution and Ag addition on the superconducting properties of Bi-2212 textured materials

B. Özçelik¹ · O. Nane¹ · A. Sotelo² · H. Amaveda² · M. A. Madre²

Received: 11 November 2016 / Accepted: 27 December 2016 / Published online: 6 January 2017
© Springer Science+Business Media New York 2017

Abstract The effect of Ag addition on the structural and superconducting properties of $\text{Bi}_2\text{Sr}_2\text{Ca}_{0.925}\text{Na}_{0.075}\text{Cu}_2\text{O}_y + x$ wt% Ag materials with $x=0, 1, 3,$ and 5 prepared by sol–gel method, followed by directional growth using the laser floating zone (LFZ) technique has been investigated. Powder XRD measurements demonstrate that all samples are composed by nearly single Bi-2212 phase. SEM micrographs and EDX results confirms that Bi-2212 is the major phase with minor amounts of a Bi-free one $(\text{Sr,Ca})\text{CuO}_2$ and metallic Ag. According to the magnetic results, Ag does not modify the superconducting critical temperature, T_c , but significantly increases the magnetic hysteresis loop area. The magnetic critical current density is maximum in the 3 wt% Ag containing samples, due to the larger grain clusters found in these samples, reaching 2.1×10^5 A/cm² at 10 K. Moreover, Ag addition also improves the rods mechanical properties, determined by three point bending tests. The highest bending stress is also reached in the 3 wt% Ag samples.

1 Introduction

BSCCO superconductor family are generally described using the $\text{Bi}_2\text{Sr}_2\text{Ca}_{n-1}\text{Cu}_n\text{O}_x$ formula, where $n=1, 2,$ or $3,$ presenting T_c 's of about 20, 85 and 110 K, respectively [1, 2], usually called Bi-2201, Bi-2212 and Bi-2223,

respectively. Since their discovery, in order to better understand their structural and physical properties, many studies have been performed on the high-temperature ones [3–16]. From all these works, it has been found that their practical applications require high electrical transport properties at 77 K [17]. In particular, many strategies and techniques have been tested to maximize these transport properties. Some of them consist in the preparation of highly homogeneous precursors with small particle sizes using different synthesis techniques [18–20], the cationic substitutions or additions to raise the superconducting performances [3–10], or improving their grain alignment to raise the electrical transport properties due to the reduction of the number of low-angle junctions [21]. The main techniques used to obtain very well aligned grains along the conducting direction are the sinter-forging [22] and the laser floating zone (LFZ) [23–26] techniques. J_c values higher than 5000 A/cm² have obtained by a modified LFZ technique in thick rods having very well oriented crystals with their c -axis perpendicular to the current flow direction and strong grain boundaries [27]. One of the main advantages of this method is that the materials can be rapidly grown due to the large thermal gradient at the solid–liquid interface [28]. A second advantage is the absence of crucible, avoiding external contamination of samples during the processing.

In previous works, the effect of Na-substitution on the structural and physical properties of Bi-2212 was studied in detail. The optimum Na-content to obtain the maximum amount of Bi-2212 phase and the best electric properties was determined as 0.075 [3, 9, 29, 30]. Due to the ceramic nature and the poor mechanical characteristics of *HTc* materials, they have strong limitations for technological applications. Some attempts to improve their mechanical properties have been performed by means of Ag addition

✉ B. Özçelik
ozcelik@cu.edu.tr

¹ Department of Physics, Faculty of Sciences and Letters,
Çukurova University, 01330 Adana, Turkey

² ICMA (CSIC-Universidad de Zaragoza), María de Luna, 3,
50018 Zaragoza, Spain

on BSCCO compounds [11], raising, at the same time, the grains electrical connectivity. As a consequence of both improvements, the aim of this work is to study the influence of Ag addition on the microstructure and physical properties in the $\text{Bi}_2\text{Sr}_2\text{Ca}_{0.925}\text{Na}_{0.075}\text{Cu}_{2+\delta}$ system textured using the laser floating zone (LFZ) technique.

2 Experimental

$\text{Bi}_2\text{Sr}_2\text{Ca}_{0.925}\text{Na}_{0.075}\text{Cu}_2\text{O}_x + x \text{ wt\% Ag}$ ($x=0, 1, 3,$ and 5) polycrystalline precursors were prepared from Bi_2O_3 ($\geq 99.9\%$, Aldrich), SrCO_3 (98%, Panreac), CaCO_3 ($\geq 99\%$, Aldrich), Na_2CO_3 ($\geq 99.99\%$, Aldrich), CuO (98%, Panreac) and Ag ($\geq 99\%$, Aldrich) commercial powders by a sol–gel method via nitrates. They were weighed in the appropriate proportions, and dissolved in a mixture of HNO_3 (Fluka, PA) and distilled water. To the clear blue solution, citric acid (99.5%, Panreac) and ethylene glycol (99%, Panreac) were added dropwise in the adequate proportions. Solvent evaporation has been slowly performed at 110°C until a pale blue dry gel has been formed. Further heating at 350°C decomposes the organic material by selfcombustion, leading to a brownish fine powder which was subsequently calcined twice, at 750 and 800°C for 12 h, with an intermediate milling to decompose the alkaline-earth carbonates. The thermally treated powders were cold isostatically pressed in form of cylinders (between 2 and 3 mm diameter) at 200 MPa. These green ceramics were used as feed in a directional solidification process performed in a LFZ installation [25]. The textured bars were obtained using a continuous power Nd:YAG laser ($\lambda=1064 \text{ nm}$), under air, at a growth rate of 30 mm/h and 18 rpm relative rotation between seed and feed. After the melt-grown processes, very homogeneous geometrically bars were obtained ($\sim 2 \text{ mm}$ diameter and 120 mm length). On the other hand, as it is well known Bi-2212 ceramic presents incongruent melting, producing different secondary phases as Bi-2201, CaCuO_2 , or $(\text{Sr,Ca})\text{CuO}_2$ [31] after solidification. As a consequence, after the texturing process, it is necessary to perform a thermal treatment in order to form the Bi-2212 superconducting phase [32, 33] from the secondary ones. This annealing process was performed under air, and consisted in two steps: 60 h at 860°C , followed by 12 h at 800°C and, finally, quenched in air to room temperature.

Structural studies of textured ceramic samples were performed by using a Rigaku D/max-B X-ray powder diffractometer ($\text{CuK}\alpha$ radiation) with 2θ ranging between 3 and 80° . Microstructural characterization was performed on longitudinal polished sections of samples using a field emission scanning electron microscope (FESEM, Zeiss Merlin) equipped with an energy dispersive spectroscopy

(EDX) system. Magnetic measurements were carried out in a Quantum Design PPMS system. Mechanical characterization of samples has been performed measuring the flexural strength by three-point bending test using an Instron 5565 universal testing machine with a 10 mm loading span fixture and a punch displacement speed of $30 \mu\text{m}/\text{min}$. At least 5 samples of each composition have been measured in order to minimize measurement errors.

3 Results and discussion

Powder XRD patterns of all samples (between 5 and 65° , for clarity) are displayed in Fig. 1. As it can be seen, the most intense peaks (labeled by +) are associated to Bi-2212 phase as the major one. The peak observed at around 38.2° (shown by *) corresponds to the (111) diffraction plane of metallic Ag [34] which can be easily observed in the 3 and 5 wt% Ag containing samples. On the other hand, the crystal symmetry is not modified by Ag addition being, in all samples, a pseudo-tetragonal structure with $a-b \approx 5.43 \text{ \AA}$ and $c \approx 30.83 \text{ \AA}$, which is in good agreement with the Bi-2212 phase crystal parameters [35].

SEM micrographs performed in longitudinal polished sections are shown in Fig. 2. As it can be easily observed in the pictures, all samples are composed by a mixture of different contrasts associated, through EDS, to different phases. Major contrast in all samples is the grey one (indicated by #1) and corresponds to the superconducting $\text{Bi}_2\text{Sr}_2\text{Ca}_{0.9}\text{Na}_{0.03}\text{Cu}_2\text{O}_y$. Dark grey and white ones are the Bi-free $(\text{Sr,Ca})\text{CuO}_2$ (#2), and Bi-2201 (#3) secondary phases, respectively. Moreover, in samples with high Ag addition (3, and 5 wt%) two new contrasts can be identified,

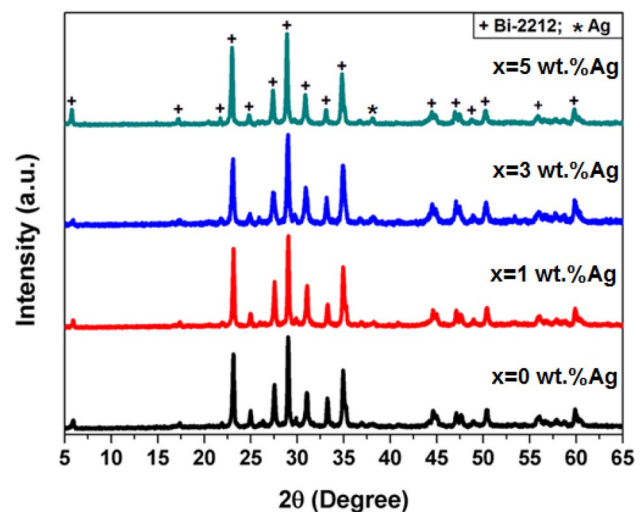
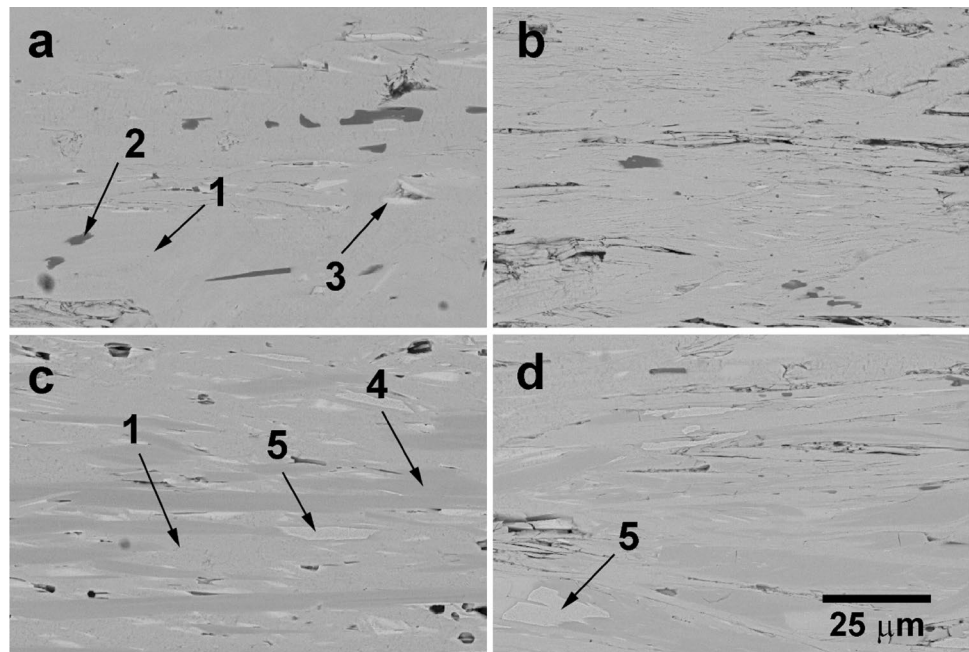


Fig. 1 XRD patterns of all samples. Peaks corresponding to the Bi-2212 and Ag phases are indicated by + and *, respectively

Fig. 2 Representative SEM micrographs of longitudinal polished sections of **a** 0 wt% Ag; **b** 1 wt% Ag; **c** 3 wt% Ag; **d** 5 wt% Ag samples. Numbers indicate the different phases: (1) $\text{Bi}_2\text{Sr}_2\text{Ca}_{0.9}\text{Na}_{0.03}\text{Cu}_2\text{O}_y$; (2) $(\text{Sr,Ca})\text{CuO}_2$; (3) Bi-2201; (4) $\text{Bi}_2\text{Sr}_2\text{Ca}_{0.9}\text{Na}_{0.06}\text{Cu}_2\text{O}_y$; (5) metallic Ag



a medium grey (#4) with $\text{Bi}_2\text{Sr}_2\text{Ca}_{0.9}\text{Na}_{0.06}\text{Cu}_2\text{O}_y$ composition and a grey one (#5) which is associated to metallic Ag. When observing these microstructures in detail, it can be observed that Ag addition clearly modifies the final microstructure of samples. These important changes are due to modifications in the molten zone promoted by the formation of isolated liquid Ag drops distributed all around the melt which produce modifications in the solidification interphase. It has been already reported that Ag addition to the pure Bi-2212 leads to the formation of an eutectic melt with lower melting temperature than the pure compounds [36, 37]. As a consequence, if the solidification temperature is lower than the pure material one, the temperature gradient between the external and the internal part of the rods is decreased leading to better aligned grains. This trend is followed until 3 wt% Ag content, decreasing for higher Ag content due to the fact that liquid Ag content is much larger and higher temperature is reached in the melt, increasing the radial gradient and, consequently, the grains misalignment.

Figure 3 shows the magnetization curves, as a function of temperature, obtained under 50 Oe applied magnetic field perpendicular to the fibers growth direction. The use of higher magnetic field than usual in a ZFC mode measurement for high- T_C superconductors has been made in order to get deeper information about the general samples texture. As it can be seen in the graph, the critical onset temperatures, T_C , corresponding to the diamagnetic transition are around 92 K in all cases, in agreement with previous works which showed that Ag does not modify T_C values [11]. In addition, the magnetization curve for 3 wt% Ag

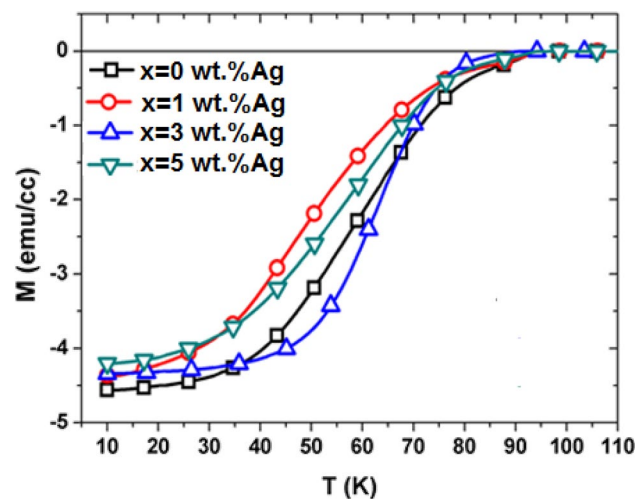


Fig. 3 Magnetization against temperature, as a function of Ag content, measured under 50 Oe applied field

samples clearly confirms the SEM observations, showing better quality, homogeneity, and grain alignment than the other ones.

Figure 4 illustrates the magnetic hysteresis loops measured at 10 K, between ± 9 T applied magnetic field perpendicular to the growth direction. The general behavior of these hysteresis curves indicates that magnetization values are strongly dependent of Ag-content. Furthermore, the reversible and symmetrical shapes of loops imply that pinning mechanism occurs by bulk pinning rather than surface and/or geometrical barriers at low fields. Moreover, the M-H loops for the 3 and 5 wt% Ag samples are larger

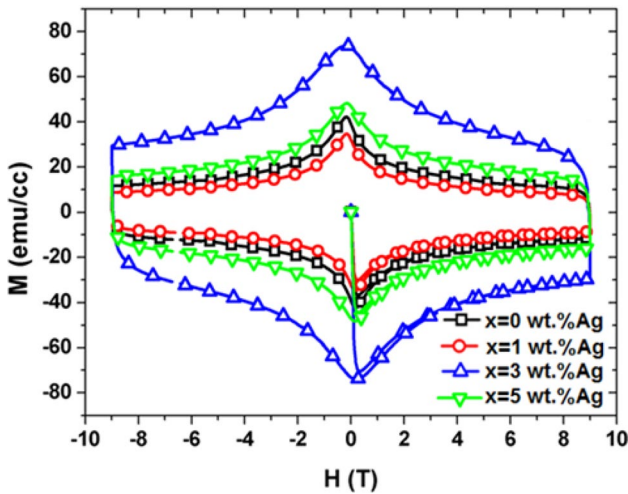


Fig. 4 M–H curves for all samples measured at 10 K

than the obtained for the pure ones. It is worth to mention that larger hysteresis loops and higher magnetization values lead to a higher intra-grain critical current density values. As a consequence, it should be expected that these samples present better transport properties than the other ones. Furthermore, Ag addition improves the microstructure of the Bi-2212 samples, reducing the porosity and increasing their mechanical properties, as well as improving the electric and magnetic properties, both at self-field and in applied magnetic fields.

The magnetic hysteresis loops measured at different temperatures for the 3 wt% Ag samples (for clarity) are given in Fig. 5. As it can be observed in the graph, the samples behavior is the typical found in Bi-2212 materials, the

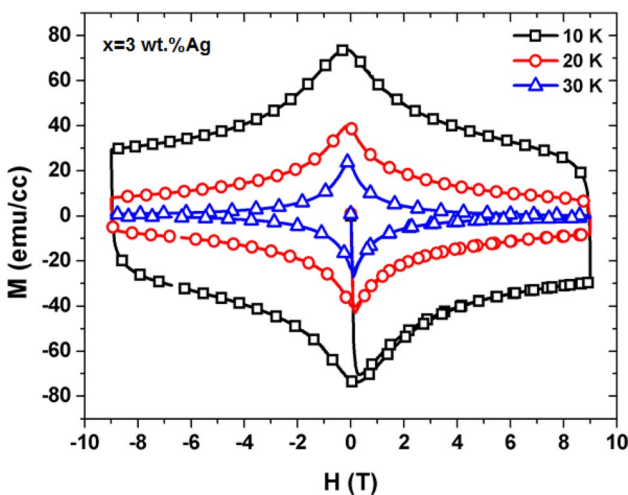


Fig. 5 M–H curves for the 3 wt% Ag samples measured at 10, 20, and 30 K

hysteresis loops area is decreased when the temperature is raised. It is well-known that due to the pinning effects and the large volume of the superconducting regions, the magnetic field penetration becomes difficult at low temperatures. But, at higher temperatures, the applied fields begin to significantly penetrate into the samples due to the decrease of the superconducting regions and the weakening of grain connectivity with increasing temperature. This is probably the reason for the decrease in the width of the magnetic hysteresis loops above 10 K [38].

The intragranular critical current density, J_c , values of samples were calculated from the hysteresis data measured at 10 K, using the Bean’s model [39].

$$J_c = 30 \frac{\Delta M}{d} \tag{1}$$

where J_c is the critical current density in ampères per square centimeter, $M = M_+ - M_-$ is measured in electromagnetic units per cubic centimeter, and d is the thickness of the sample. The obtained results, as a function of the applied magnetic field, are presented in Fig. 6. In the plot, it can be observed that J_c values gradually decrease when the magnetic field is increased in all cases. Moreover, high Ag addition (3, and 5 wt% Ag) contributes to the pinning mechanism, raising these values, when compared with the undoped sample, being the highest ones for the 3 wt% Ag samples. The reasons for these high J_c values can be explained taking into account that Na contributes to a higher content of the superconducting phase, increases grain sizes, and slightly improves grain orientation [3, 9]. These larger and better oriented grains imply a lower number of grain boundaries and a decrease of angles between adjacent grains, leading to higher J_c values.

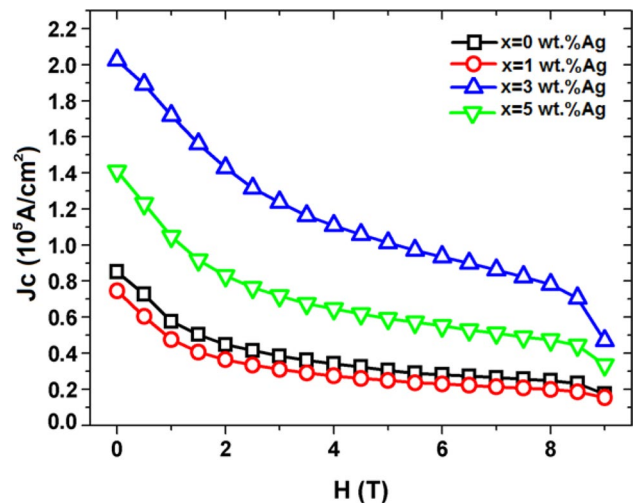


Fig. 6 Calculated critical current densities, J_c , of all samples at 10 K, as a function of the applied field

Moreover, besides the Na effect, Ag addition improves electrical grains connectivity, as discussed above. While $\text{Bi}_2\text{Sr}_2\text{Ca}_{0.925}\text{Na}_{0.075}\text{Cu}_2\text{O}_y$ (without Ag) sample possesses a relatively low J_c ($0.9 \times 10^9 \text{ A/cm}^2$), it is raised for the 3 wt%Ag samples to $2.1 \times 10^9 \text{ A/cm}^2$. Further Ag addition decreases J_c but it is still around $1.4 \times 10^9 \text{ A/cm}^2$, which is higher than the measured in the Ag-free samples. Taking into account these values, it can be suggested that $\text{Bi}_2\text{Sr}_2\text{Ca}_{0.925}\text{Na}_{0.075}\text{Cu}_2\text{O}_y + 3 \text{ wt}\% \text{Ag}$ composition samples are suitable for practical applications on systems working at low temperatures.

In order to better understand the vortex pinning nature in the 3 wt%Ag samples, the Dew-Hughes model [40] has been used to analyze the experimentally obtained data. The model consists in representing the reduced pinning force F_p/F_{pmax} versus the reduced field H/H_{max} (shown in Fig. 7) and fitting the results using the $f_p(F_p/F_{pmax}) = b^p(1-b)^q$ equation. For high- T_c superconductors, three theoretical models [41] are used to analyze the experimental data, represented by blue continuous, and red and green dotted lines for the normal surface pinning, normal point pinning and Δk pinning, respectively. These theoretical equations are given as:

$$f_p(b) = 25 - 16b^{-1/2}(1 - b/5)^2; \text{ normal surface pinning} \quad (2)$$

$$f_p(b) = 9/4b(1 - b/3)^2; \text{ normal point pinning} \quad (3)$$

$$f_p(b) = 3b^2(1 - 2b/3); \Delta k \text{ pinning} \quad (4)$$

As it can be seen in the graph, the experimental results for 3 wt%Ag sample are well-matched with the normal

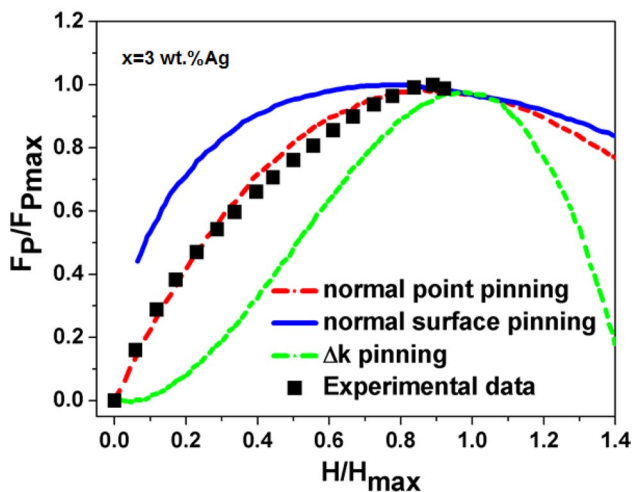


Fig. 7 Reduced Pinning Force F_p/F_{pmax} versus reduced applied field H/H_{max} for the 3 wt% Ag samples. Blue continuous, and dotted red and green lines represent the $25/16b^{-1/2}(1-b/5)^2$, $9/4b(1-b/3)^2$, and $3b^2(1-2b/3)$ theoretical models, respectively. (Color figure online)

point pinning (dotted red line) in the whole measured field range.

Finally, mechanical properties of samples, measured through the three point bending test, are presented in Fig. 8, where mean flexural strength values, together with their standard error, are represented as a function of Ag content. As it can be observed in the figure, all Ag containing samples possess higher strength than the Ag-free ones, in agreement with previous works in similar systems [42, 43]. Moreover, Ag addition also decreases the results dispersion, reflected in lower standard error. These improvements can be associated to the silver particles shape and position, as they are filling the intergranular holes between superconducting grains. As a consequence, silver provides a plastic-flow region when the samples are subjected to stresses, resisting crack propagation by deflecting it, as it has been previously reported in close ceramic systems [11]. On the other hand, the amount of Ag to reach the highest mechanical properties is higher in this work than in previous ones [11], probably due to the effect of Na-doping which produces larger plate-like grains [9, 44] with low mechanical performances in the ab plane. As a consequence, the required amount of Ag to reinforce these grain boundaries is increased.

4 Conclusion

In this study, $\text{Bi}_2\text{Sr}_2\text{Ca}_{0.925}\text{Na}_{0.075}\text{Cu}_2\text{O}_8 + x \text{ wt}\% \text{Ag}$ with $x = 0, 1, 3, \text{ and } 5$ ceramics have been prepared by a sol-gel method, followed by directional growth using the laser floating zone (LFZ) technique. XRD patterns have demonstrated that all samples are composed by nearly single

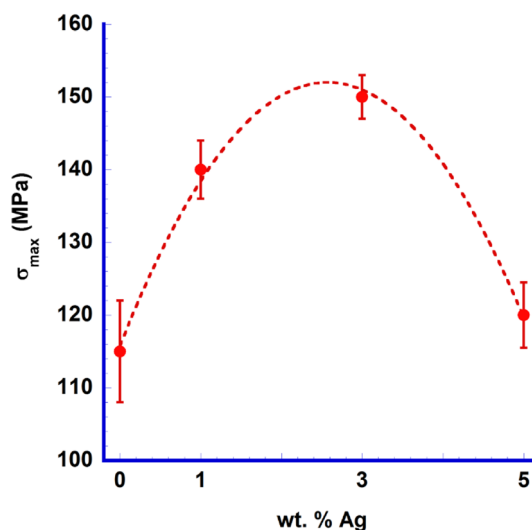


Fig. 8 Mean flexural strength, together with their standard error, versus Ag-content

Bi-2212 phase. The SEM micrographs and EDX results corroborate that Bi-2212 is the major phase with minor amounts of Bi-free (Sr,Ca)CuO₂ and metallic Ag. According to *M-T* results, Ag does not modify the superconducting critical temperature, T_c , but raises the magnetic hysteresis loop area. The critical current density is drastically improved for 3 wt% Ag-addition, due to the larger grain clusters formed in these samples. The highest intragranular J_c value was calculated as 2.1×10^5 A/cm² at 10 K for the 3 wt% Ag samples. It is also observed that this amount of Ag improves the mechanical properties of the samples. All these results clearly point out that Ag-addition in the adequate amount can raise, in an important manner, the superconducting and mechanical properties of Bi-2212 textured samples.

Acknowledgements This work is supported by Research Fund of Çukurova University, Adana, Turkey, under Grant Contracts No: FBA-2016-6626. M. A. Madre acknowledges MINECO-FEDER (Project ENE2014-52105-R) for funding. M. A. Madre and A. Sotelo acknowledge the MINECO-FEDER (Project MAT2013-46505-C3-1-R) and the Gobierno de Aragón (Consolidated Research Group T12) for financial support. Authors acknowledge the use of Servicio General de Apoyo a la Investigación-SAI, Universidad de Zaragoza.

References

1. C. Michel, M. Hervieu, M.M. Borel, A. Grandin, F. Deslands, J. Provost, B. Raveau, Z. Phys. B. **86**, 421 (1987)
2. H. Maeda, Y. Tanaka, M. Fukutumi, T. Asano, Jpn. J. Appl. Phys. **27**, 209 (1988)
3. B. Özçelik, M. Gürsul, A. Sotelo, A. M. Madre, J. Mater. Sci. **26**, 441 (2015)
4. B. Özçelik, C. Kaya, H. Gündoğmuş, A. Sotelo, M.A. Madre, J. Low Temp. Phys. **174**, 136 (2014)
5. A. Özaslan, B. Özçelik, B. Özkurt, A. Sotelo, M.A. Madre, J. Supercond. Nov. Magn. **27**, 53 (2014)
6. H. Gündoğmuş, B. Özçelik, B. Özkurt, A. Sotelo, M. A. Madre, J. Supercond. Nov. Magn. **26**, 111 (2013)
7. V. Lennikov, B. Özkurt, L. A. Angurel, A. Sotelo, B. Özçelik, G. F. de la Fuente, J. Supercond. Nov. Magn. **26**, 947 (2013)
8. O. Nane, Z. Özçelik, A. Sotelo, M.A. Madre, Ceram. Int. **42**, 3418 (2016)
9. O. Nane, B. Özçelik, H. Amaveda, A. Sotelo, M.A. Madre, Ceram. Int. **42**, 8473 (2016)
10. B. Özçelik, M. Gürsul, A. Sotelo, A. M. Madre. J. Mater. Sci. **25**, 4476 (2014)
11. A. Sotelo, M. Mora, M.A. Madre, J.C. Diez, L.A. Angurel, G.F. de la Fuente, J. Eur. Ceram. Soc. **25**, 2947 (2005)
12. M. Mora, A. Sotelo, H. Amaveda, M.A. Madre, J. C. Diez, L.A. Angurel, G. F. de la Fuente, Bol. Soc. Esp. Ceram. V. **44**, 199 (2005)
13. G.F. de la Fuente, A. Sotelo, Y. Huang, M.T. Ruiz, A. Badia, L.A. Angurel, F. Lera, R. Navarro, C. Rillo, R. Ibañez, D. Beltran, F. Sapiña, A. Beltran, Physica C **185**, 509 (1991)
14. C. Kaya, B. Ozcelik, B. Ozkurt, A. Sotelo, M.A. Madre, J. Mater. Sci. **24**, 1580 (2013)
15. A. Sotelo, G.F. de la Fuente, F. Lera, D. Beltran, F. Sapiña, R. Ibañez, A. Beltran, M.R. Bermejo, Chem. Mater. **5**, 851 (1993)
16. A. Sotelo, P. Majewski, H.S. Park, F. Aldinger, Physica C. **272**, 115 (1996)
17. M. Chen, L. Donzel, M. Lakner, W. Paul, J. Eur. Ceram. Soc. **24**, 1815 (2004)
18. V. Rouessac, J. Wang, J. Provost, G. Desgardin, J. Mater. Sci. **31**, 3387 (1996)
19. A. Sotelo, H. Szillat, P. Majewski, F. Aldinger, Supercond. Sci. Technol. **10**, 717 (1997)
20. A. Sotelo, Sh. Rasekh, M. A. Madre, J.C. Diez, J. Supercond. Nov. Magn. **24**, 19 (2011)
21. D. Shi, *High temperature superconducting materials science and engineering*. (Pergamon Press, Oxford, 1995)
22. V. Garnier, R. Caillard, A. Sotelo, G. Desgardin, Physica C **319**, 197 (1999)
23. F.M. Costa, Sh. Rasekh, N.M. Ferreira, A. Sotelo, J.C. Diez, M.A. Madre, J. Supercond. Nov. Magn. **26**, 943 (2013)
24. Y. Huang, G.F. de la Fuente, A. Sotelo, A. Badia, F. Lera, R. Navarro, C. Rillo, R. Ibañez, D. Beltran, F. Sapiña, A. Beltran, Physica C **185–189**, 2401 (1991)
25. M.F. Carrasco, F.M. Costa, R.F. Silva, F. Gimeno, A. Sotelo, M. Mora, J.C. Diez, L.A. Angurel, Physica C **415**, 163 (2004)
26. F.M. Costa, N.M. Ferreira, Sh. Rasekh, A.J.S. Fernandes, M.A. Torres, M.A. Madre, J.C. Diez, A. Sotelo, Cryst. Growth Des. **15**, 2094 (2015)
27. J.C. Diez, L.A. Angurel, J.I. Pena, E. Martinez, G.F. de la Fuente, R. Navarro, R. Bol. Soc. Esp. Ceram. V. **36**, 159 (1997)
28. R.S. Feigelson, D. Gazit, D.K. Fork, T.H. Geballe, Science **240**, 1642 (1988)
29. B. Özçelik, M. Gürsul, A. Sotelo, A. M., Madre. J. Mater. Sci. **26**, 2830 (2015)
30. M. Gürsul, A. Ekicibil, B. Özçelik, M.A. Madre, A. Sotelo, J. Supercond. Nov. Magn. **28**, 1913, (2015)
31. M. Mora, A. Sotelo, H. Amaveda, M.A. Madre, J.C. Diez, F. Capel, J.M. Lopez-Cepero, J. Eur. Ceram. Soc. **27**, 3959 (2007)
32. F.M. Costa, R.F. Silva, J.M. Vieira, Physica C **323**, 23 (1999)
33. O. Nane, B. Özçelik, D. Abukay, J. Alloy. Compd. **566**, 175 (2013)
34. G. Becherer, R. Iffland, Naturwissenschaften **41**, 471 (1954)
35. X. Zhao, W. Wu, X. Sun, X.G. Li, Physica C **320**, 225 (1999)
36. A. Sotelo, B. Ozcelik, H. Amaveda, A. Bruned, M.A. Madre, Ceram. Int. **41**, 14276 (2015)
37. P. Majewski, A. Sotelo, H. Szillat, S. Kaesche, F. Aldinger, Physica C **275**, 47 (1997)
38. D. Yazıcı, B. Özçelik, M.E. Yakıncı, J. Low Temp. Phys. **163**, 370–379 (2011)
39. C.P. Bean, Phys. Rev. Lett. **8**, 250 (1962)
40. D. Dew-Hughes, Philos. Mag. **30**, 293 (1974)
41. D. Sharma, R. Kumar, V.P.S. Awana, Ceram. Int. **39** 1143–1152 (2013)
42. A. Sotelo, M.A. Torres, G. Constantinescu, Sh. Rasekh, J.C. Diez, M.A. Madre, J. Eur. Ceram. Soc. **32**, 3745 (2012)
43. F. Kahraman, M.A. Madre, Sh. Rasekh, C. Salvador, P. Bosque, M.A. Torres, J.C. Diez, A. Sotelo, J. Eur. Ceram. Soc. **35**, 3835 (2015)
44. B. Ozkurt, J. Supercond. Nov. Magn. **27**, 2407 (2014).